IEEE Access
Multidisciplinary | Rapid Review | Open Access Journal

Received August 10, 2021, accepted August 29, 2021, date of publication August 31, 2021, date of current version September 10, 2021.

Digital Object Identifier 10.1109/ACCESS.2021.3109504

Impact of Wind Variation on the Measurement of Wind Turbine Inertia Provision

SAM HARRISON[1], PANAGIOTIS N. PAPADOPOULOS[1], (Member, IEEE), RICARDO DA SILVA[2], ANTHONY KINSELLA[2], ISAAC GUTIERREZ[2], AND AGUSTI EGEA-ALVAREZ[1], (Member, IEEE)

[1]Department of Electronic and Electrical Engineering, University of Strathclyde, Glasgow G1 1XQ, U.K.
[2]ScottishPower Renewables, Glasgow G2 5AD, U.K.

Corresponding author: Sam Harrison (sam.harrison@strath.ac.uk)

This work was supported by the Engineering and Physical Sciences Research Council under Grant EP/L016680/1.

ABSTRACT Wind turbine (WT) control is being adapted to enable inertia provision that supports network frequency on short timescales. Measuring the inertia contribution from wind turbines is critical to asses the provision of the service as well as understand the WT operation. However, inertia measurement methods disagree on the impact of the wind and how to approximate its effects. This paper uses data from a ScottishPower Renewables (SPR) test of a grid connected wind farm to highlight that wind can impact inertia provision and that external network power measurements are unable to measure the inertia. Two proposals are made to improve inertia measurements. First, the International Electrotechnical Commission (IEC) industrial standard for WT inertia measurement is adapted, and secondly, an alternate method using system identification is proposed that considers characteristics of the WT's dynamic response. The measurement methods from the literature and the proposals are assessed using the output of time-domain WT models to find the sensitivity of their accuracies to variations in the wind, frequency, and control-setting conditions. The methods from the literature are inaccurate during variable wind conditions but the proposed approaches improve the accuracy. The findings of the sensitivity study are then validated by applying the measurement methods to the SPR wind farm experimental data and confirm that the proposed system identification method is the most accurate measurement approach.

INDEX TERMS Inertia provision, power system stability, system identification, wind energy generation.

I. INTRODUCTION

The inertia of synchronous generators (SGs) acts as an energy storage that instantaneously responds to rapid imbalances in power generation and demand. The inertial power constrains the rate of change of frequency (ROCOF) on the network to low levels during the first instances after disturbances [1]. SGs are being displaced by energy sources that are interfaced with power converters, which remove the electromagnetic coupling between generator and grid. Wind turbines (WTs) are one of the most common displacing technologies [2]. The displacement of SGs reduces the energy storage available to rapidly balance power and risks severe frequency variations [3]. Low inertia levels and frequency instability are affecting systems with high penetration of power converters such as Ireland and Great Britain, which have to curtail power converter interfaced generation to maintain system security [4], [5].

Power converter control has the ability to respond quickly to system changes [6] and to operate flexibly throughout different conditions [7]. The rapid response allows converters to emulate SG behaviour and provide a similar inertial response. Inertia provision is possible from many energy sources interfaced by a converter, including: WTs [8], energy storage systems (ESSs) [9], and interconnectors [10].

The conventional WT Current Control strategy is grid following (GFL) as it uses a phase-locked loop (PLL) to synchronise the power output with the grid [11]. A simple ROCOF dependent power adjuster is added to the control, which varies the output during a frequency event [8]. The strategy faces complications in low-inertia systems, however, as the PLL can struggle to synchronise with rapidly changing grid angles [11]. An alternative synchronisation method could be used such as the frequency-locked loop using multiple second order generalised integrators [12].

The associate editor coordinating the review of this manuscript and approving it for publication was Dong Shen.

TABLE 1. Table of abbreviations.

Abbreviation	Meaning
ENTSO-E	European Network of Transmission System Operators for Electricity
ESS	Energy storage system
FDF	Frequency-divider formula
GFL	Grid-following/follower
GFM	Grid-forming/former
IEC	International Electrotechnical Commission
KE	Kinetic energy
MPPT	Maximum power point tracking
NG ESO	National Grid Electricity System Operator
PCC	Point of common connection
PLL	Phase-locked loop
PMSG	Permanent-magnet synchronous generator
PMU	Phasor measurement unit
ROCOF	Rate of change of frequency
SG	Synchronous generator
SO	System operator
SPR	ScottishPower Renewables
VSM	Virtual synchronous machine
WF	Wind farm
WT	Wind turbine

Grid forming control offers an alternative that sets an internal voltage, rather than following the grid [13]. Virtual synchronous machine (VSM) is a family of grid forming controllers (GFM) inspired by the dynamics of SGs that are capable of desirable functions such as inertia provision [14], black start capability [15], and stable operation in weak grids [16]. The strategies include different representations of the swing equation that vary the converter output in response to grid power imbalances [17]–[19]. Generally, the equivalent inertia constant is defined by the control strategy's parameters and sets the magnitude of the inertial response.

Accurate inertia measurement is a key requirement to enable the deployment of inertia-emulating control strategies on WTs. GB's National Grid Electricity System Operator (NG ESO) have highlighted the need for increased monitoring of GFM converter devices [20]. The measurement enables the verification and understanding of the inertial provision that is essential for a cost-effective and reliable service. With the help of accurate measurement the provision can be regulated in whichever form the System Operator (S0) desires. ScottishPower Renewables (SPR) applied a VSM control strategy to the grid connected Dersalloch Wind Farm (WF) [21] and note that a simple inertia measurement using external frequency and power at the terminals of the WF is inaccurate due to coinciding wind changes. [21] considered improving the inertia measurement accuracy by using an internal control signal to find the power baseline that the inertial response can be identified above. This baseline should represent the power output in steady state conditions, as if the WF experienced the same wind and control settings but no frequency disturbance. The data from the grid-connected experiment are assessed in more detail in Section II and show that the internal signals commonly used for inertia measurement do not account for all of the wind-driven power variations.

Alternatively, the IEC industrial standard for measuring WT inertia, detailed in the IEC standard 61400-21-1:2019 [22], suggests using an Available Active Power signal as a power baseline to remove the wind's impact. The IEC method uses a wind speed measurement to find the Available Active Power baseline, which is then compared with the total power injected at the WT's point of common connection (PCC) to find the inertial power change. The IEC method is reconstructed for clarity in the Appendix in Fig. 8. Although the IEC standard does not define Available Active Power, it is thought to be equivalent to the NG ESO definition of Power Available: a low bandwidth estimation of the energy in the wind that can be extracted by a WT [23]. The Power Available signal will be used in place of the Available Active Power throughout this paper.

There are two main reasons that Power Available may not be an appropriate baseline for inertia measurement. First, inertia measurement needs to be able to resolve close to instantaneous dynamics [14]. The Power Available does not account for the mechanical inertia of the turbine, which determines the rate at which the WT's electrical power output can respond to changes in the power in the wind (on the order of 10s of seconds for modern WTs). The signal cannot resolve WT output on timescales <10 seconds, which overlaps with the inertial response. Secondly, higher level controls may move the WT power set point away from the Power Available in the wind. For example, if the WT rotor speed is effected sub-optimally the power set point will be adjusted to ensure safe operation and eventual recovery [24]. Alternatively, WTs might be ordered to curtail their output below the power in the wind according to an energy balancing market [25].

Several other measurement tools have been proposed in the literature to identify the inertia provided by converter-interfaced devices, such as WTs. Discrete time-domain phasor-measurement unit (PMU) power and frequency measurements are used to fill a finite-difference approximation of the swing equation and equate the doubley-fed induction generator WTs with an equivalent SG [26]. The order of the finite-difference approximation of the swing equation is increased to improve the estimation accuracy in [27]. Unlike [21], [22], both approaches in [26], [27] assume the slower mechanical WT system does not vary on inertial timescales so approximate the mechanical power to be equal to the electrical power at the start of the frequency event. By neglecting the wind's impact the inertia estimators can be simplified and operated using only external information from the WT terminals. However, the accuracy of this assumption has not been validated for type-4 WTs that are subject to wind variations.

The frequency-divider formula (FDF) [28] is used to develop a generator rotor speed dynamic state estimator using external power and frequency measurements and knowledge of the system admittance [29]. Then, the Regulating Power is defined using the FDF as the component of active power that affects the grid frequency [30]. Both the generator rotor speed and Regulating Power parameters are incorporated in

TABLE 2. Review of inertia measurement techniques discussed in Section I.

Reference	Description	Application	Operational timeframe	Considering converter based inertia	Approximation for effects of wind	Error subject to wind variability
[22]	Mean inertial power boost above mean base power	IEC Standard WT inertia test	Offline (pre-connection)	Yes	Power available baseline	N/A
[26]	Discretised swing equation using discrete PMU measurements	Individual device (WT) inertia estimation	Online (given accurate disturbance detection)	Yes	Initial mechanical power baseline	N/A
[27]	Adapted [26] with higher order discretised swing equation	Individual device (WT) inertia estimation	Online (given accurate disturbance detection)	Yes	Initial mechanical power baseline	N/A
[31]	Heuristic estimator utilising Regulating Power signal and estimated bus frequency deviation	Individual device (SG & converter) inertia estimation	Online	Yes	Frequency and second derivative of frequency deadband thresholds	$< \|17.25\|$ %
[32]	Swing equation based method using polynomial curve fitted power and frequency signals	Inertia estimation of SGs on microgrids with high penetration of renewables	Online	No	N/A	N/A
[33]	System identification of separate SG and GFL converter models	SG and GFL converter inertia estimation	Online	Yes	N/A	N/A
[36]	Identification of transfer function from PMU measurements	Power system inertia estimation	Online	No	Initial mechanical power baseline	N/A
[37]	Adapted [36] using estimated ROCOF from swing equation	Power system inertia estimation	Online	No	Initial mechanical power baseline	N/A
[38]	Autoregressive model considering sum of periodic and stochastic parts	Power system inertia estimation	Online	No	Stochastic variable	< 8 %

an inertia estimator [31]. The estimator incorporates simple deadband-threshold margins to remove the impact of comparatively small wind-driven power variations relative to a large inertial response by an ESS with inertia constant $H = 40\ s$. However, a WT's inertia constant is generally an order of magnitude smaller so is more effected by the non-frequency dependent power variations. The simple deadband-threshold margins will either mask the smaller WT inertial response or be skewed by the WT's complex non-frequency dependent behaviour, such as the rotor speed recovery and wind variations.

Reference [32] develops an estimator to measure SG inertia on systems with high penetrations of renewable energy sources. The tool is assessed and finds that the rapid frequency support from GFL converters is delayed relative to the SG inertia (resulting from the use of the PLL). An inertia estimator is then developed that uses system identification to fit parameters to two separate SG and GFL converter models [33]. The estimator relates the rapid power provided by converters to inertia, but again, is affected by the complex non-frequency dependent behaviour of WTs. Moreover, the tool does not consider GFM inertia from converters, which can respond on similar timescales to SG inertia [20].

A comparison of inertia estimators agrees that SG inertia can be isolated from the delayed GFL WT's frequency-supporting power response [34] but does not consider inertia provided by GFM WTs. The slow time constant and controllable nature of the SGs allows inertia estimators to assume that the mechanical power is constant on inertial timescales [35]–[37], similar to the assumptions made for WTs in [26], [27]. However, as the penetration of converter interfaced devices increases even the SG inertia estimators have to be developed to account for the increasing impact of the converter's rapid power variations [38]. Reference [39] highlights the increased complexity for inertia measurement of energy sources interfaced by converters. Inertia measurement methods specific to the technology and control type are suggested to be developed [39], and while future work accounting for the uncertainty of renewables is encouraged, there is no explicit discussion of the wind's impact on inertia provision.

There is a clear need to define the impact of wind variation on inertia provision. The varying timescales of rapid frequency support from SGs vs GFL converters vs GFM converters has led to different approximations of the wind's impact, as shown in Table 2, which details and compares the inertia measurement methods discussed in this Section. This is a particular issue for GFM WTs, whose power output is intrinsically dependent on the wind and whose inertial-power response overlaps with both the conventional inertia from SGs and GFL converter responses. The IEC industrial standard approach for measuring WT inertia has not been validated throughout wind variations. Moreover, some approaches suggest WT inertia can be resolved using external information [10], [27] despite others suggesting the

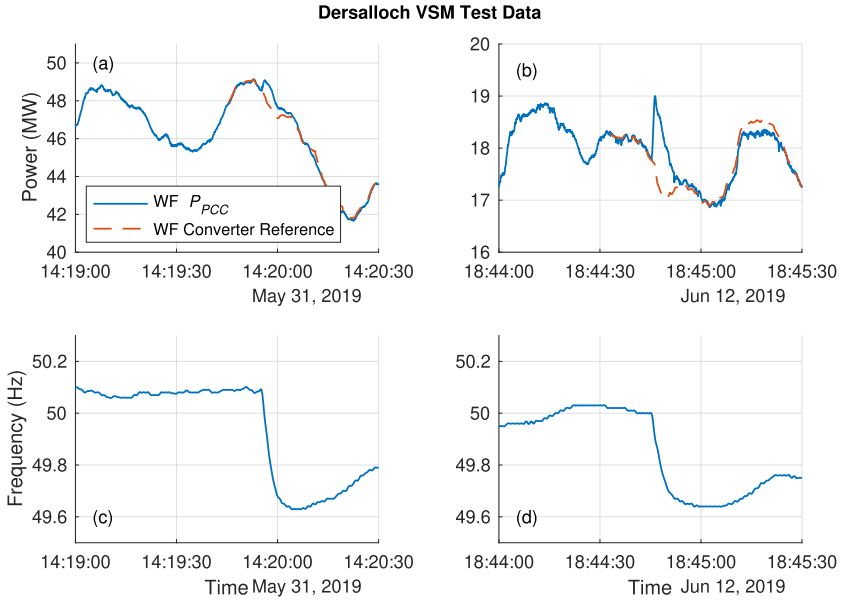

FIGURE 1. Dersalloch WF PCC power and reference power in response to two different frequency disturbances on (a) the 31st of May and (b) the 12th of June. The corresponding frequency excursions are shown in (c) and (d).

impact of wind variations will decrease the measurement accuracy [21].

This paper aims to address the uncertainty surrounding the impact of the wind's variation on WT inertia provision, and hence its measurement. The paper then offers proposals to improve inertia measurement methods. The significant contributions are:

- The use of grid-connected Dersalloch WF experimental data to assess the impact of wind on GFM inertia provision and its measurement.
- A proposal to improve the accuracy of the IEC industrial standard approach for WT inertia measurement.
- The development of an alternative GFM WT inertia measurement tool that accounts for the WT's response dynamics.
- A sensitivity analysis highlighting inertia measurements' accuracy throughout different wind, frequency, and control conditions.
- Validation of the sensitivity analysis results using the grid-connected Dersalloch WF experimental data.

II. DERSALLOCH WF INERTIA PROVISION

Data from the ScottishPower Renewables test of a grid-connected VSM at Dersalloch WF, using SiemensGamesa RE WTs, is shown in Fig. 1 during two frequency disturbances. The experimental data is used here to highlight the impact of wind on inertial response by real WTs and how it impacts the accuracy of basic inertia measurement approaches. Full analysis of the experiment is detailed in [21]. The data includes the external signals that SPR use for a conventional inertia measurement: the frequency and power at the PCC. The internal WF reference signal is also included.

Both of the frequency disturbances pictured in Fig. 1 are triggered by the tripping of the France-England Interconnector. On the 31st of May the WF is operating at a rated power of 69 MW with an equivalent inertia constant of $H = 4$ s when the interconnector trip drives a ROCOF of 0.11 Hz/s. On the 12th of June the WF is operating at a rated power of 60 MW with an equivalent inertia constant of $H = 7.5$ s, now the interconnector trip drives a ROCOF of 0.08 Hz/s.

The WF power varies due to the wind's impact during both of the pictured operational periods. The changes occur on short timescales that coincide with the timescales of the inertial response.

The inertia estimators for power systems [36], [37] and WTs [26], [27] suggest that the inertial response could be measured as the difference between the initial and boosted PCC power. The SPR experimental data can be used to compare this power change observed on the grid with that expected from the WF. Equation 1 calculates the expected response ΔP_{exp} using the WF equivalent inertia constant H, rated power S_n, and synchronous speed ω_0, and the maximum ROCOF of the frequency event $\dot{\omega}_{max}$:

$$\Delta P_{exp} = \frac{2HS_n}{\omega_0}\dot{\omega}_{max} \tag{1}$$

The expected power changes calculated using Equation 1 for each event are $\Delta P_{31/05,exp} = 1.21$ MW and $\Delta P_{12/06,exp} = 1.44$ MW, respectively. The inertial power changes measured as the difference between the initial and boosted PCC power are $\Delta P_{31/05,PCC} = 0.54$ MW and $\Delta P_{12/06,PCC} = 1.21$ MW. The measurement using only the grid power is incapable of resolving the inertial response, particularly for the event on the 31st of May that coincides

with a severe wind decrease and hence total power decrease. The measurement inaccuracy on the 31st is also affected by the low inertia constant, which drives a response that is small compared to the wind driven changes.

Instead of using the initial PCC power, the converter reference could be used to represent the inertial baseline [21], however, the reference is an internal signal that is not currently provided to the SO. Fig. 1 shows the WF power reference for both events and highlights good tracking of the PCC power outside of the frequency disturbance. Some discrepancy is visible between the PCC and reference powers during the speed recovery of the WT 15 to 30 seconds after the initiation of each event.

The inertial power changes measured as the average difference between the converter reference and the PCC power are $\Delta P_{31/05,ref} = 0.83$ MW and $\Delta P_{12/06,ref} = 1.34$ MW. The measurement using the converter reference as the baseline gives power changes closer to the expected values but still contains considerable error for the event on the 31st of May. The discrepancy between the reference and the PCC power during the speed recovery after the frequency event suggests that the internal reference used here doesn't account for the impact of all of the (non-frequency dependent) operating conditions on the power output, which is insufficient to remove all of the error from the inertia measurement.

III. PROPOSALS TO IMPROVE INERTIA MEASUREMENT

A. IMPROVEMENTS TO IEC INDUSTRIAL STANDARD

To achieve accurate inertia measurement, the IEC Standard method that was introduced in Section I needs to use a baseline that is representative of the WT's steady state operation. Power Available is expected to be unable to resolve WT output on short timescales as it fails to account for the mechanical and electrical systems between the WT rotor and the PCC. The attempts to measure inertia in Section II suggest that the initial PCC power is not an appropriate baseline either as it doesn't account for wind variations.

The maximum power point tracking (MPPT) reference is proposed to be used as the baseline in an improved IEC method. The MPPT reference is the power value that the WT attempts to track to achieve optimal operation [40]. The reference uses the rotor speed to determine the set-point so will account for any event that affects turbine operation. Assuming proper tuning of the converter, the MPPT reference equates to the PCC power during steady state conditions. It should be noted that the MPPT reference is inspired by, but distinct from, the converter reference in Section II, which didn't account for the adjusted power during the turbine speed recovery phase.

B. EQUIVALENT SWING METHOD

The IEC methodology uses a simple difference of two averages to measure the inertia. The improved IEC method may accurately measure inertia using the MPPT baseline, however, if the reference is affected by improper tuning it could introduce error to the inertia measurement. An alternative approach, the Equivalent Swing method, is proposed that derives the inertia constant from the properties of the dynamic inertial response and not just from the magnitude of the power change.

The Equivalent Swing method uses the same information as the improved IEC method: the frequency at the PCC and the inertial power change ΔP_{MPPT} (the difference between the PCC and MPPT powers). However, the measurements are input to a system identification algorithm to find the inertia constant.

$G_{SG}(s)$ describes a SG's PU inertial power output ΔP_{SG} in response to the frequency change input $\Delta\omega$:

$$G_{SG}(s) = \frac{\Delta P_{SG}(s)}{\Delta\omega(s)} = \frac{-\frac{k_d}{\omega_0}s^2 - k_s s}{s^2 + \frac{k_d}{2H}s + \frac{k_s\omega_0}{2H}} \tag{2}$$

k_d is the damping coefficient, k_s is the synchronising torque, ω_0 is the synchronous speed, and H is the inertia constant of the SG. Reference [41] highlights that the damping provided by SGs includes an external component through the damper windings, whereas, VSMs provide virtual damping exclusively through an internal path. Despite some differences in the operation of the two devices, the Equivalent Swing method assumes that the inertial response from WTs is equivalent to that from conventional SGs. A similar assumption is made when equating VSMs and SGs in [42]. The Equivalent Swing Method aims to identify the apparent synchronous inertia that is provided to the grid so compares the WT output with the SG transfer function in Equation 2 opposed to a VSM specific transfer function. This may also allow the methodology to be applied accurately to other control configurations.

Considering this assumption, the measured frequency change input to the WT $\Delta\omega$ and the measured inertial power change output by the WT ΔP_{MPPT} are proposed to be fed to the MATLAB continuos-time transfer function estimation algorithm [43]. Both the power and frequency data streams are pre-processed to remove any offset before system identification. The system identification estimates a 2nd order transfer function $G_{est}(s)$ that describes this inertial response to a frequency disturbance:

$$G_{est}(s) = \frac{\Delta P_{MPPT}(s)}{\Delta\omega(s)} = \frac{As^2 + Bs + C}{Ds^2 + Es + F} \tag{3}$$

Coefficients A, B, C, D, E, and F are the estimated parameters that represent the measured WT system. If the power change used for the identification is the exact inertial response of the WT the estimated parameters in $G_{est}(s)$ correspond to the physical parameters they represent in $G_{SG}(s)$ i.e. estimated parameter F equates to $\frac{k_s\omega_0}{2H}$.

Parameter B is an estimate of the negative synchronising torque that can be used with parameter F and the known synchronous speed to find the estimated inertia constant H_{est}:

$$H_{est} = \frac{k_s\omega_0}{2F} = \frac{-B\omega_0}{2F} \tag{4}$$

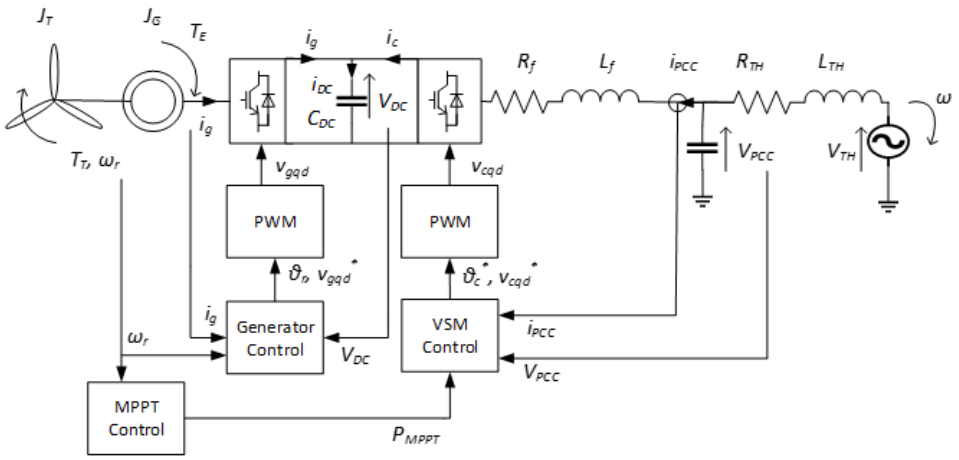

FIGURE 2. Electromechanical model of PMSG WT connected to the Thevenin Equivalent representation of the grid. The converter control blocks are also included. The constant parameter values are detailed in Table 3.

IV. SENSITIVITY ANALYSIS

A sensitivity analysis is carried out to find the accuracy of a range of the reviewed and proposed inertia measurement methods (from Sections I and III, respectively) throughout wind variations. The methods are also assessed to ensure that they are robust for different frequency events and inertia constant settings. The inertia is measured using the relevant power and frequency signals (for each measurement method) output by a model of a type four inertia providing WT. The accuracy of the methods throughout the sensitivity scenarios are defined relative to the inertia constant set in the model's control. The methods that are assessed are detailed in Section IV-A, the model is detailed in Section IV-B, and the sensitivity scenarios are described in Section IV-C.

A. MEASUREMENT METHODS

Four measurement methods are subject to the sensitivity analysis. The first method is the Standard IEC Method, which measures the inertial response as the mean power change from the onset of the frequency disturbance to the nadir between the PCC power and the Power Available baseline. Power Available is calculated as:

$$P_{Avlb} = \frac{1}{2}\rho\pi R^2 C_p u^3 \tag{5}$$

ρ is the air's density in the WT rotor radius R, C_p is the power coefficient, and u is the wind speed. The second measurement method is a variation of the IEC method, which uses the initial PCC power as the baseline, and is named the Initial Power IEC Method. This method is representative of the existing external information available for inertia measurement and of the approximation made for the wind in some of the inertia estimators in the literature [26], [27], [36], [37]. The third IEC method uses the mean MPPT reference during the frequency event as the baseline, as proposed in Section III-A. This method is referred to as the Improved IEC Method.

Finally, the Equivalent Swing Method, proposed in Section III-B, is subject to the sensitivity analysis.

B. WIND TURBINE AND NETWORK MODEL

A generic 3 MW direct drive WT is modelled (and pictured in Fig. 2 in terms of mechanical, electrical, and control components). The full electromechanical model is necessary to capture the interaction of both the wind and the frequency [40]. All turbine, grid, and control parameters can be found in Table 3.

TABLE 3. WT, network, and control parameters.

Wind turbine		Network	
R (m)	43.5	SCR	10
ρ (kg/ m^3)	1.225	L_{TH} (μH)	50.2
J_T (kg m^2)	1.3x10^7	R_{TH} (mΩ)	1.6
J_G (kg m^2)	1.4x10^6	C_f (mF)	3.0
p (pairs)	60	L_f (μH)	50.5
ψ (Wb)	22.3	R_f (mΩ)	1.6
L_{sd}=L_{sq} (mH)	4.0		
R_s (mΩ)	5.4	Control	
C_{DC} (F)	0.5	V_{DC}^* (V)	800
c_1	1	ζ	0.31
c_2	39.52	v_n^* (V)	563.4
c_3	0		
c_4	0		
c_5	0		
c_6	2.04		
c_7	14.47		
c_8	0		
c_9	0		

The WT rotor is connected to a permanent magnet synchronous generator (PMSG) via a single-mass drive-train model, as outlined in [44]. The PMSG is modelled as described in [45] and is linked to the network via a back-to-back voltage-source converter.

The generator converter uses a conventional current control strategy, whose active current reference is set by a DC link controller. The network converter uses a 2nd order VSM that

directly feeds a voltage angle and magnitude to the waveform modulation, similar to the control topology described in [46]. The VSM damping ζ is set to 0.31 and the inertia constant H is set according to the sensitivity scenario, as detailed in Section IV-C. The VSM uses a voltage controller to regulate the network voltage.

The VSM power reference is fed by the MPPT scheme described in [40]. The MPPT power (P_{MPPT}) is dependent on the WT mechanical parameters including: the gearbox ratio $GBR = 1$, the rotor speed ω_r, and the WT characteristic parameters $[c_1 \dots c_9]$:

$$P_{MPPT} = \frac{1}{GBR} K_{MPPT} \omega_r^3 \tag{6}$$

$$K_{MPPT} = \frac{1}{2}\rho\pi R^5 \frac{c_1 \left(c_2 + c_6 c_7\right)^3 e^{-\frac{(c_2 + c_6 c_7)}{c_2}}}{c_2^2 c_7^4} \tag{7}$$

C. SENSITIVITY SCENARIOS

The sensitivity scenarios are grouped according to frequency, wind, and inertia constant settings. Frequency and wind scenario labels (FX and UX, respectively) refer to a specific magnitude and rate of change of disturbance while inertia constant scenario labels (HX) simply refer to the equivalent inertia constant.

All of the frequency disturbances, which initiate at $t = 4$ s, are shown in Table 4. The magnitude of the frequency change scenarios are: 0.1 Hz (representing a small deviation), 1 Hz (representing the maximum permissible steady state frequency deviation for European Grid operators [47]), and 5 Hz (representing a large deviation considered in the ENTSO-E document describing future grid needs [48]). The ROCOF of the frequency disturbance scenarios are: 0.1 Hz/s (representing a low ROCOF), 0.5 Hz/s (representing a threshold that activates Loss-of-Mains protection relays [49]), and 2.5 Hz/s (also derived from the ENTSO-E document describing future grid needs [48]).

TABLE 4. Frequency disturbance sensitivity scenarios.

Event	Deviation (Hz)	ROCOF (Hz/s)
$F1$	0.1	0.1
$F2$	1	0.5
$F3$	5	0.5
$F4$	1	2.5
$F5$	5	2.5

Wind speed is constant at $u = 8.5$ m/s until a disturbance is forced at $t = 2$ s. The wind speed is kept below rated speed as the study is interested in the variation of power with wind. A wind step-up or step-down du is applied, equivalent to the maximum 20 second gust speed for each of the IEC's turbulent wind classes [50] (Equation 8 [24]):

$$du = u_{mean}\left(1 + \left[1 + I0.42ln\left(\frac{3600}{T_G}\right)\right]\right) \tag{8}$$

u_{mean} is the average wind speed, I is the turbulence intensity, and T_G is the gust period. Constant and smaller wind steps are also applied to see the effects of less severe wind environments. All of the wind disturbances are detailed in Table 5.

TABLE 5. Wind disturbance sensitivity scenarios. Multiple wind scenarios are grouped according the rate of change of wind speed.

Event	Deviation (m/s)	Rate (m/s^2)
$U1$	0	0
$U2$ *to* $U5$	[1 2.2 2.6 3]	0.5
$U6$ *to* $U9$	[1 2.2 2.6 3]	1
$U10$ *to* $U13$	[1 2.2 2.6 3]	1.5
$U14$ *to* $U17$	[-1 -2.2 -2.6 -3]	-0.5
$U18$ *to* $U21$	[-1 -2.2 -2.6 -3]	-1
$U22$ *to* $U25$	[-1 -2.2 -2.6 -3]	-1.5

Finally, the control parameters of the network side converter are varied. The VSM inertia constant is varied between three settings, all of which maintain stable converter operation but result in increasingly large inertial responses. The range of inertia constants are detailed in Table 6.

TABLE 6. Equivalent inertia constant sensitivity scenarios.

Configuration	Inertia Constant (s)
$H1$	1
$H2$	2
$H3$	3

V. RESULTS AND ANALYSIS

A. IMPACT OF WIND ON INERTIA PROVISION

Fig. 3 shows the Power Available for the WT (red line) and the corresponding PCC Power output (blue line) during three example scenarios from the full range of analysed conditions. Each scenario is subject to frequency disturbance $F2$ and inertia constant $H1$ but different wind conditions: a) step-down ($U25$), b) constant ($U1$), and c) step-up ($U13$).

The PCC power differs during the varying wind conditions despite the constant frequency disturbance and inertia constant. This confirms the findings of the Dersalloch tests that inertia provision is affected by the wind [21] and that it needs to be properly accounted for in measurement methods.

The impact of wind will affect the net inertial response on the grid. Consider an under-frequency event: the total power level will be reduced as the wind decreases (below rated speed) and the magnitude of the inertial response is diminished. Above rated, constant, or rising wind speeds will not reduce the net inertial power injected to the grid during under-frequency events, however, any upwards power variations will reduce the transparency of the inertial response if inaccurate measurement methods are used.

B. STANDARD IEC METHOD ACCURACY

The mean of the Power Available (red dash) and the PCC power (blue dash) during the frequency events (between $t = 4$ *to* 6 s for the pictured frequency scenario $F2$) are also included in Fig. 3. The two mean values represent the baseline

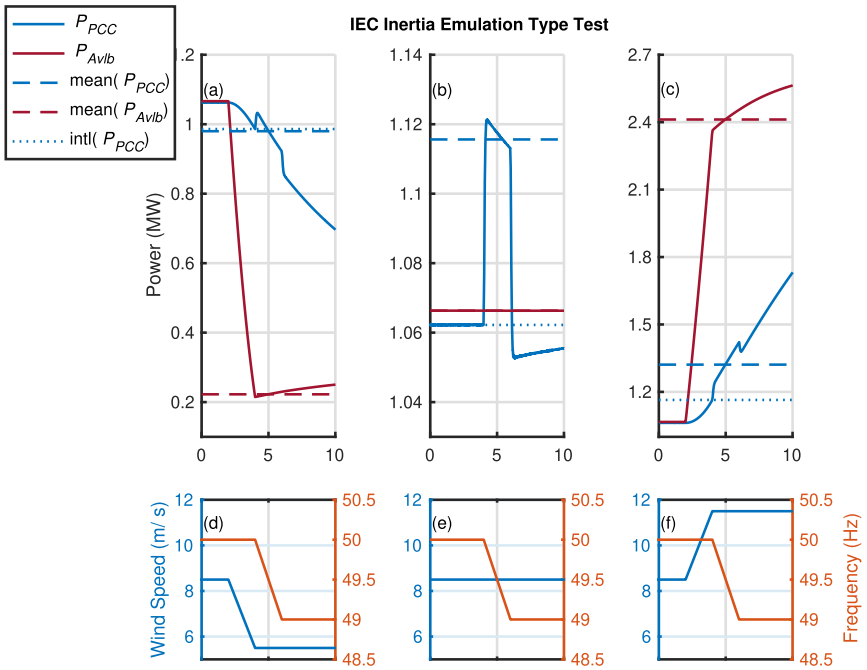

FIGURE 3. Power signals and their representative values used to carry out the Standard and Initial Power IEC Methods for (a) step-down (*U*25), (b) constant (*U*1), and (c) step-up (*U*13) wind conditions. The inertia constant configuration is *H*1 and the frequency scenario is *F*2 for all of the pictured responses. The corresponding wind and frequency conditions are shown in subplots (d), (e), and (f).

and boosted inertial power values used by the Standard IEC Method.

Power Available is shown to overestimate the wind's impact on the WT baseline (Fig. 3). The baseline changes instantaneously with the wind and at a greater rate than the PCC power. During the wind step-down this results in a low baseline and overestimation of the inertial response (Fig. 3 a)). During the wind step-up this results in a high baseline and underestimation of the inertial response to be negative (Fig. 3 c)).

The Standard IEC Method remains unable to capture the WT dynamics fully even during constant wind speeds; the base power is overestimated by around 10 kWs (Fig. 3 b)). The overestimation results from the inability of the Power Available to account for the transformation of the power in the wind to the electrical power injected to the PCC.

A particularly important feature of this process is the transformation of the WT's rotational kinetic energy (KE) into electrical energy during the inertial response. By removing KE the WT rotor is decelerated. As discussed in Sections III and IV-A the WT operating point is determined by the rotor speed. The rotor deceleration will reduce the power baseline and, therefore, the total power injected to the PCC during the frequency event, irrespective of the constant wind. Power Available does not account for this baseline variation so the Standard IEC Method measures a reduced inertial response.

Table 7 shows the range of errors (the estimated inertia constant H_{est} as a percentage of the constant set in the control)

TABLE 7. Range of inertia measurement errors (%) for tested methods across the sensitivity scenarios.

	Inertia Constant Measurement Error (%)		
	Minimum	Average (absolute)	Maximum
Standard IEC Method	-9800	830	6100
Initial Power IEC Method	-420	87	740
Improved IEC Method	-17	6.2	-0.60
Equivalent Swing Method	-0.42	0.050	0.20

recorded throughout the sensitivity study using the Standard IEC Method. The inappropriate Power Available baseline results in inaccuracies approaching 10000%. Fig. 4 a) shows the Standard IEC Method error for frequency disturbance *F*2 as the wind and inertia constant scenarios vary. The measurement is most inaccurate when the inertia provision coincides with extreme wind step-ups or step-downs. The inaccuracy translates to a larger percentage error for small power changes resulting from low inertia constants.

C. INITIAL POWER IEC METHOD ACCURACY

The Initial Power IEC Method using the mean PCC power as the boosted value (blue dash) and the initial PCC power as the baseline (blue dot) achieves accurate inertia measurement for constant wind conditions (Fig. 4 b)). However, the method

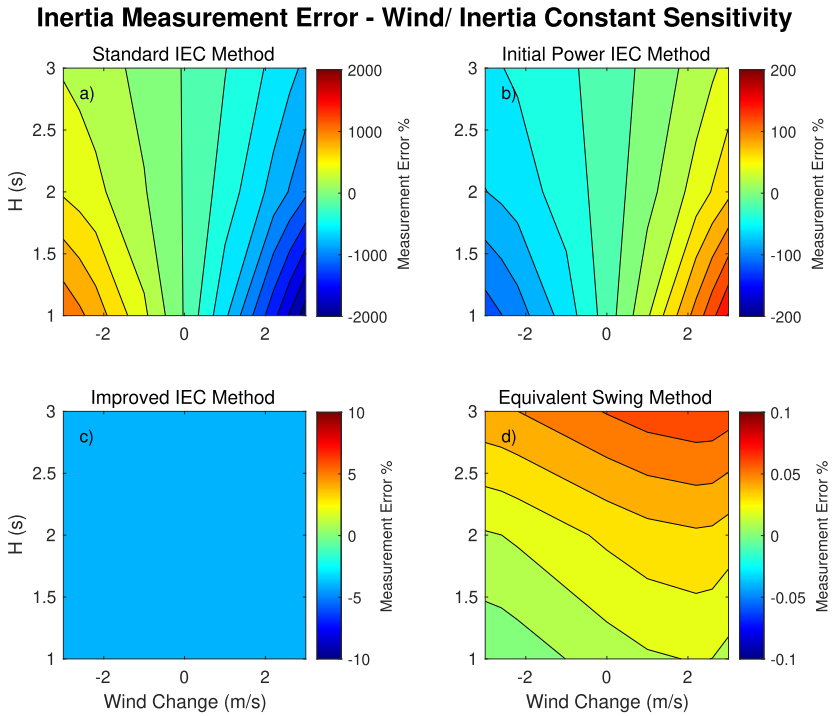

FIGURE 4. Inertia measurement error for frequency scenario $F2$ as the wind condition and inertia constant changes. Subplots exhibit the error for different methods: a) Standard IEC method, b) Initial power IEC method, c) Improved IEC method, and d) Equivalent swing method.

fails to account for the impact of the wind after the initiation of the frequency event. For example, as the wind speed decreases in Fig. 3 a), the mean PCC power decreases and the apparent inertial power is reduced (to be negative) relative to the constant initial PCC power baseline. The inertia underestimation for wind step-downs and overestimation for wind step-ups is visible in Fig. 4 b).

The Initial Power IEC Method achieves an absolute error of 11% during the constant wind case pictured in Fig. 3 b). This is similar to the errors reported by the other individual device estimators in the literature that use an initial PCC power baseline during constant wind conditions: 8% [26] and 4% [27]. Inertia measurement methods that approximate the impact of the wind in this manner should also expect similar inaccuracies to those recorded for the Initial Power IEC Method when subject to variable wind conditions (between −420% and 740%).

D. IMPROVED IEC METHOD ACCURACY

Fig. 5 shows the MPPT reference (green line) and the PCC power output (blue line) during a coinciding frequency disturbance ($F2$) and wind step-up ($U13$). The MPPT tracks the steady state PCC power accurately. The inertial power change identified using the MPPT baseline is similar, but not identical, to the Regulating Power signal [29] that is used in the FDF based inertia estimator in [31]. The inertial power is the WT power that responds to changes in frequency above the MPPT reference, however, variations in the remaining

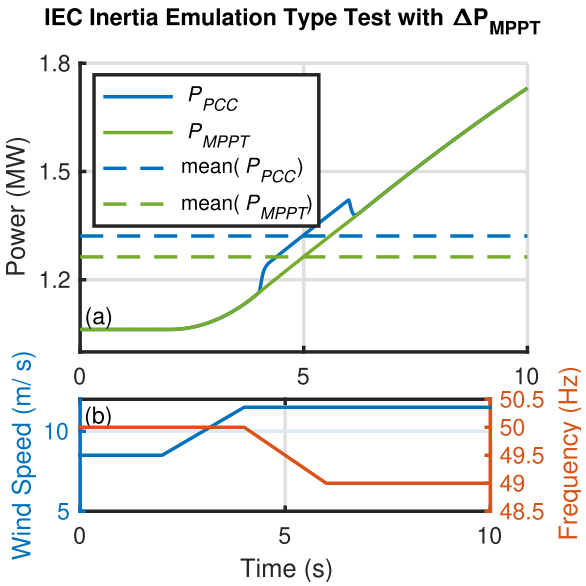

FIGURE 5. (a) Power signals used for the Improved IEC method and (b) the corresponding wind and frequency conditions.

portion of the WT output set by the MPPT reference will also affect the network frequency.

The Improved IEC Method achieves good measurement accuracy; the maximum absolute error for the entire range of sensitivity scenarios is 17% (Table 7). The accuracy of the

Improved IEC Method is independent of wind disturbance and inertia constant, depicted by the constant error contour in Fig. 4 c).

Although the FDF based inertia estimator considers the variation of the wind it is not applied to an inertia providing WT [31]. The FDF based estimator is applied to a large inertia ESS, whose inertial response is easier to resolve, and who does not experience the complex WT dynamics such as the transformation of KE to electrical power. In contrast, the Improved IEC Method has been proven to measure WT inertia accurately and can improve the existing industrial standard.

E. EQUIVALENT SWING METHOD ACCURACY

Fig. 6 shows the estimated output of a WT inertial response using the system identification stage of the Equivalent Swing Method. The estimated output depicts the accuracy of the estimation by passing the measured frequency (the input to the WT system $\Delta\omega$) through the identified transfer function (the representation of the WT system $G_{est}(s)$).

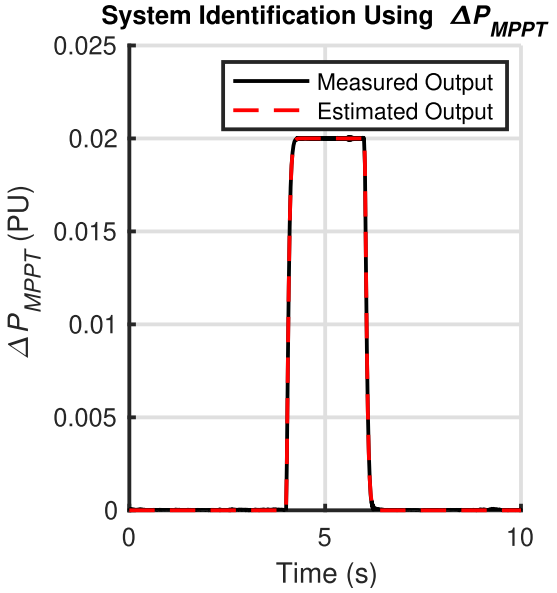

FIGURE 6. System identification estimated output compared to measured MPPT inertial power change output for wind step down ($U25$). The inertia constant setting is $H1$ and the frequency scenario is $F2$.

The identification is independent of the wind conditions due to the use of the MPPT baseline. The system identification process achieves a fit of at least 97% between the measured power output and the estimated output for all of the sensitivity scenarios, proving the accuracy of the approximation of the WT inertial response to a 2nd order system.

Using these well fitted models, the Equivalent Swing Method is the most accurate of the tested inertia measurement methods. The maximum absolute error is constrained below 0.50% (Table 7). Fig. 4 d) shows higher error for wind step-ups and for higher inertia constants but the consistently small error means the trends are not significant.

The accurate inertia measurement proves the applicability of the Equivalent Swing methodology to VSM WTs but the approach may face issues when applied to WTs that do not explicitly emulate SGs. However, the accurate relation of the SG swing equation to the inertial response of a Current Control based strategy in [27] suggests that the SG equivalence may be appropriate beyond VSMs. The steady state equivalence between VSMs and GFM droop controllers has been discussed in [46], [51], which suggests that the SG equivalence could remain accurate for other GFM converters as well.

F. SENSITIVITY TO FREQUENCY DISTURBANCE

The measurement methods are subject to frequency disturbances with varying frequency change magnitudes and ROCOFs to ensure they remain robust throughout a range of events. Fig. 7 shows the inertia measurement sensitivity to the frequency disturbance properties for a wind step-down ($U25$) and inertia constant $H1$. Frequency disturbance $F1$ (with frequency deviation 0.1 Hz and ROCOF 0.1 Hz/s) is plotted independently from the contour as it doesn't share its low frequency change or ROCOF with other scenarios. The Standard and Initial Power IEC Methods show sensitivity to the ROCOF. The inaccuracy introduced to both methods by the baselines contributes to a larger error when the ROCOF and inertial power change are smaller. The direction of the error is dependent on the given wind step-up and the respective overestimation (Standard IEC Method) and underestimation (Initial Power IEC Method) of the wind's impact by each method. For example, during the pictured frequency event $F1$, wind step-down $U25$, and inertia constant $H1$, the Standard IEC Method overestimates the inertia measurement by 6100%, whereas, the Initial Power IEC Method underestimates the same scenario by 270%.

The methods that incorporate the MPPT have reduced dependency on the frequency disturbance properties compared to the Standard and Initial Power IEC Methods. However, the Improved IEC Method regularly overestimates frequency event $F4$, which has a deviation of 1 Hz and a ROCOF of 2.5 Hz/s, by around 10% more than other events. The Equivalent Swing Method is generally least accurate for either frequency event $F4$ or $F1$, but again, the low error magnitude means this is not a weakness in the measurement approach.

VI. APPLICATION OF METHODS TO DERSALLOCH EXPERIMENTAL DATA

The inertia measurement methods that are assessed throughout the sensitivity study are applied to the data from the SPR Dersalloch inertia provision test. The objective is to validate the accuracy of each method when applied to real WT systems.

The measurement methodologies used in this Section are the same as those described in Section IV-A other than a few key approximations that had to be made due to the availability of the experimental data. The Standard IEC Method uses an

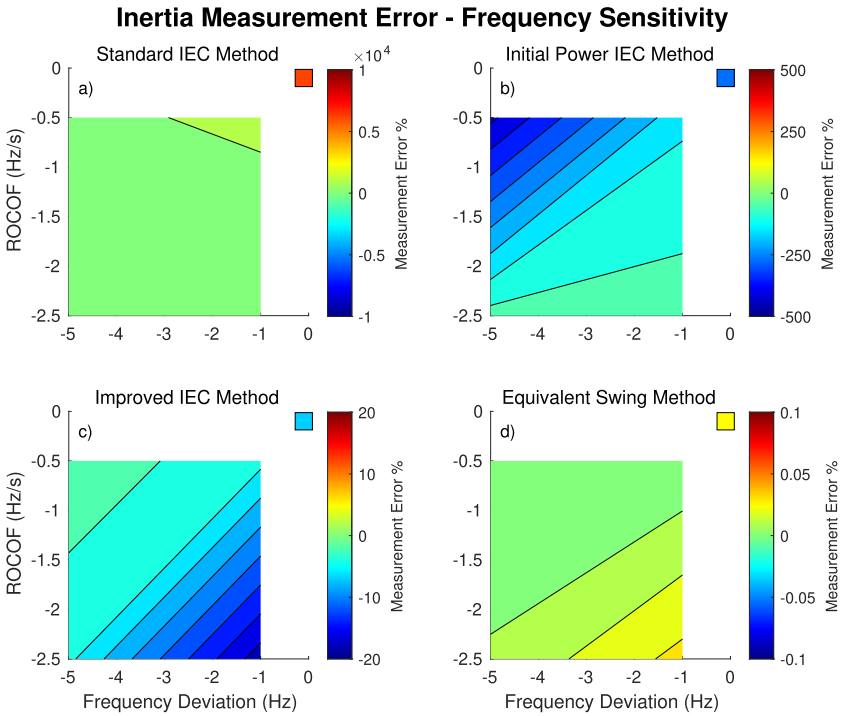

FIGURE 7. Inertia measurement error for a wind step-down (*U*25) and inertia constant *H*1 as the frequency change magnitude and ROCOF vary. Subplots exhibit the error for different methods: a) Standard IEC Method, b) Initial Power IEC Method, c) Improved IEC Method, and d) Equivalent Swing Method. Frequency disturbance *F*1 is plotted as an independent point from the contour.

approximated Power Available for the entire wind farm. The MPPT reference is replaced with the wind farm converter reference for both the Improved IEC and Equivalent Swing Methods. The inertia constant measured by each method is recorded as a percentage error of the inertia constant of the wind farm during the given disturbance. Although the exact structure of the WT control is unknown, the wind farm is known to operate with an inertia constant of $H_{31/05} = 4$ s on the 31st of May and of $H_{12/06} = 7.5$ s on the 12th of June.

Table 8 shows the inertia constant measurement errors using each method for both disturbances. In general, the Dersalloch data confirms the findings of the sensitivity study. The Standard IEC Method is the least accurate approach. The Power Available baseline overestimates the impact of the wind, which is exhibited by the large overestimation of the inertial response (340%) on the 31st of May that coincides with a severe drop in wind. The underestimation of the inertia constant by 160% during the same disturbance by the Initial Power IEC Method confirms its underestimation of the wind's impacts. The less severe wind conditions on the 12th of June do not provide as conclusive results for the Standard and Initial Power IEC Methods.

TABLE 8. Range of inertia measurement errors (%) for tested methods when applied to the Dersalloch experimental data.

	Inertia Constant Measurement Error (%)	
	31/05	12/06
Standard IEC Method	340	-150
Initial Power IEC Method	-160	-100
Improved IEC Method	-33	-25
Equivalent Swing Method	-12	13

The Improved IEC Method that was proposed in Section III-A achieves better inertia measurement accuracy than the existing measurement methods. However, the use of the alternate reference as the baseline introduces more error (between 25% and 33%) than is observed when using the MPPT reference throughout the sensitivity study (constrained below 17%). The sub-optimal baseline signal also reduces the accuracy of the Equivalent Swing method for the Dersalloch data. However, the system identification approach is able to capture the dynamic response of the wind farm and constrains the error to be less than 13% during both events. By extending the inertia measurement to consider properties of the dynamic response the Equivalent Swing Method is able to remove some of the error introduced to the Improved IEC Method by the alternate converter reference baseline. The Equivalent Swing Method is confirmed to be the most accurate approach to measure WT inertia.

VII. CONCLUSION

This paper assesses the impact of wind variations on inertia providing wind turbines. Existing methods available to measure WT inertia disagree how to approximate the wind's

effects on the rapid power injections. Particular focus is paid to the IEC industrial standard, which is thought to use an inappropriate Power Available baseline to measure inertia from. The need for internal information to accurately measure inertia, such as the Power Available, is also assessed.

The analysis of data from a test at a grid connected ScottishPower Renewables wind farm confirms that inertia provision is affected by wind variability and that it should not be neglected from inertia measurement. The simple approach using the difference between the initial and boosted external PCC measurements was incapable of accurately measuring the inertia, particularly during large wind variations.

A type 4 wind turbine model is subject to a sensitivity study. Four measurement methods are applied to the simulated data to assess their accuracy throughout varying wind, frequency, and inertia constant conditions. The methods that are assessed are: the Standard IEC Method and the Initial Power IEC Method, from the literature, and the Improved IEC Method and the Equivalent Swing Method, the two methods proposed in this paper.

When the Standard IEC method uses the Power Available as the baseline it is found to be very inaccurate (errors as large as −9800%). The Power Available overestimates the impact of the wind on the short timescales and may not be appropriate for inertial analysis, despite being proposed to increase transparency of wind turbines on longer timescales. The sensitivity study finds the Initial Power IEC Method to underestimate the wind's impact during the inertial response. The error in both methods is worse when the ROCOF is low and the wind's impact masks the small inertial response more. The results of the sensitivity study confirm the findings of the grid connected wind farm that external data is insufficient to measure WT inertia, however, the internal Power Available is not the appropriate solution.

The IEC Method is proposed to be improved by incorporating the maximum power point tracking reference as the baseline. The reference is an alternative internal signal that provides an accurate representation of the WT steady state conditions and enables accurate inertia measurement (maximum error of −17%). An alternative approach to the IEC method is proposed that accounts for the full inertial response dynamics. This alternative, the Equivalent Swing Method, is the most accurate inertia measurement across all of the sensitivity scenarios (error less than 0.50%). The tested measurement methods are then applied to the Dersalloch Wind Farm experimental data to confirm their accuracy for real-world wind turbines. The Equivalent Swing Method is also found to be the most accurate inertia measurement method for the experimental data but as the MPPT reference is not available the maximum error extends to 12%.

APPENDIX
IEC STANDARD INERTIA MEASUREMENT

The IEC inertia measurement method is reconstructed in Fig. 8 from the IEC standard [22]. The wind speed, spanning five seconds before to five seconds after the frequency

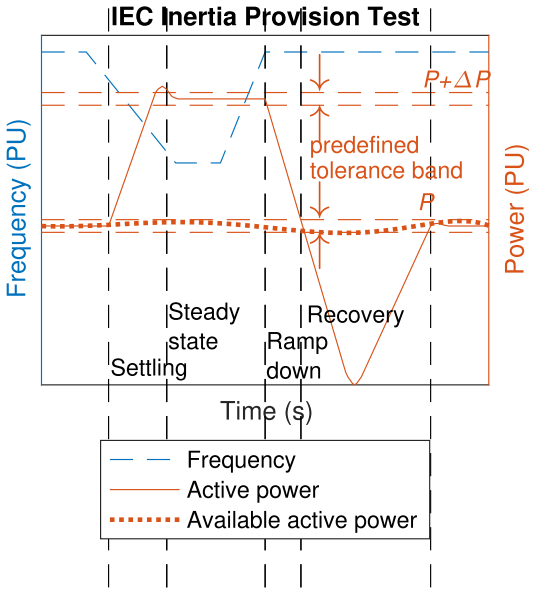

FIGURE 8. IEC WT inertia test methodology, reconstructed from [22]. The power and frequency signals, inertial power bands, and operating time periods are included.

event, is used to find the Available Active Power. The difference during the frequency event between the power measured at the terminals of the WT and the Available Active Power gives the inertial power, which can be compared with the frequency measured at the terminals of the WT to determine the inertial properties.

REFERENCES

[1] P. Kundur, J. Paserba, V. Ajjarapu, G. Andersson, A. Bose, C. Canizares, N. Hatziargyriou, D. Hill, A. Stankovic, C. Taylor, T. Van Custem, and V. Vittal, "Definition and classification of power system stability IEEE/CIGRE joint task force on stability terms and definitions," *IEEE Trans. Power Syst.*, vol. 19, no. 3, pp. 1387–1401, May 2004.

[2] I. Komusanac, G. Brindley, and D. Fraile, "Wind energy in Europe in 2019," Wind Eur., Brussels, Belgium, Tech. Rep., Feb. 2020.

[3] A. Adrees, P. N. Papadopoulos, and J. V. Milanovic, "A framework to assess the effect of reduction in inertia on system frequency response," in *Proc. IEEE Power Energy Soc. Gen. Meeting (PESGM)*, Boston, MA, USA, Jul. 2016, pp. 1–5.

[4] *Annual Renewable Energy Constraint and Curtailment Report 2018*, Non-Tech. Summary, EirGrid, SONI, Dublin, Ireland, Belfast, U.K., May 2019.

[5] M. Joos and I. Staffell, "Short-term integration costs of variable renewable energy: Wind curtailment and balancing in Britain and Germany," *Renew. Sustain. Energy Rev.*, vol. 86, pp. 45–65, Apr. 2018.

[6] F. Milano, F. Dörfler, G. Hug, D. J. Hill, and G. Verbič, "Foundations and challenges of low-inertia systems (invited paper)," in *Proc. Power Syst. Comput. Conf. (PSCC)*, Dublin, Ireland, Jun. 2018, pp. 1–25.

[7] J. Matevosyan, V. Vital, J. O'Sullivan, R. Quint, B. Badrzadeh, T. Prevost, E. Quitmann, D. Ramasubramanian, H. Urdal, S. Achilles, J. MacDowell, and S. H. Huang, "Grid-forming inverters: Are they the key for high renewable penetration?" *IEEE Power Energy Mag.*, vol. 17, no. 6, pp. 89–98, Nov. 2019.

[8] J. Morren, S. W. H. de Haan, W. L. Kling, and J. A. Ferreira, "Wind turbines emulating inertia and supporting primary frequency control," *IEEE Trans. Power Syst.*, vol. 21, no. 1, pp. 433–434, Feb. 2006.

[9] H. Beltran, S. Harrison, A. Egea-Àlvarez, and L. Xu, "Techno-economic assessment of energy storage technologies for inertia response and frequency support from wind farms," *Energies*, vol. 13, p. 3421, Jul. 2020.

[10] M. Zhang, X. Yuan, and J. Hu, "Inertia and primary frequency provisions of PLL-synchronized VSC HVDC when attached to islanded AC system," *IEEE Trans. Power Syst.*, vol. 33, no. 4, pp. 4179–4188, Jul. 2018.

[11] *Performance of Phase-Locked Loop Based Converters*, Nat. Grid ESO, Warwick, U.K., 2017.
[12] P. Rodríguez, A. Luna, I. Candela, R. Teodorescu, and F. Blaabjerg, "Grid synchronization of power converters using multiple second order generalized integrators," in *Proc. 34th Annu. Conf. IEEE Ind. Electron.*, Orlando, FL, USA, Nov. 2008, pp. 755–760.
[13] P. Christensen, M. Seidel, S. Engelken, T. Knueppel, A. Krontiris, K. Wuerflinger, T. Bulo, J. Jahn, S. Salehi, I. Theologitis, B. Weise, H. Urdal, A. Egea-Alvarez, and J. Fortmann, "High penetration of power electronic interfaced power sources and the potential contribution of grid forming converters," ENTSO-E Tech. Group High Penetration Power Electron. Interfaced Power Sources, Brussels, Belgium, Tech. Rep., 2020.
[14] Y. Lin, J. H. Eto, B. B. Johnson, J. D. Flicker, R. H. Lasseter, H. N. V. Pico, G.-S. Seo, B. J. Pierre, and A. Ellis, "Research roadmap on grid-forming inverters," Nat. Renew. Energy Lab., Golden, CO, USA, Tech. Rep., 2020.
[15] *Black Start From Non-Traditional Generation Technologies*, Nat. Grid ESO, Warwick, U.K., Jun. 2019.
[16] R. Ierna, J. Zhu, H. Urdal, A. J. Roscoe, M. Yu, A. Dysko, and C. D. Booth, "Effects of VSM convertor control on penetration limits of non-synchronous generation in the GB power system," in *Proc. 15th Wind Integr. Workshop*, Nov. 2016, p. 8.
[17] H.-P. Beck and R. Hesse, "Virtual synchronous machine," in *Proc. 9th Int. Conf. Elect. Power Qual. Utilisation*, Barcelona, Spain, Oct. 2007, pp. 1–6.
[18] Q.-C. Zhong and G. Weiss, "Synchronverters: Inverters that mimic synchronous generators," *IEEE Trans. Ind. Electron.*, vol. 58, no. 4, pp. 1259–1267, Apr. 2011.
[19] M. Yu, A. J. Roscoe, C. D. Booth, A. Dysko, R. Ierna, J. Zhu, N. Grid, and H. Urdal, "Use of an inertia-less virtual synchronous machine within future power networks with high penetrations of converters," in *Proc. Power Syst. Comput. Conf. (PSCC)*, Genoa, Italy, Jun. 2016, pp. 1–7.
[20] *GC0137: Minimum Specification Required for Provision of GB Grid Forming (GBGF) Capability (Formerly Virtual Synchronous Machine/ VSM Capability)*, WorkGroup Consultation, Nat. Grid ESO, Warwick, U.K., Mar. 2021.
[21] A. Roscoe, P. Brogan, D. Elliott, T. Knueppel, I. Gutierrez, J.-C. P. Campion, and R. Da Silva, "Practical experience of operating a grid forming wind park and its response to system events," in *Proc. 18th Int. Wind Integr. Workshop*, Dublin, Ireland, Oct. 2019, p. 7.
[22] *Wind Energy Generation Systems. Part 21-1: Measurement and Assessment of Electrical Characteristics—Wind Turbines*, IEC Standard 61400-21-1:2019, BSI Standards Limited 2019, Brussels, Belgium, 2019.
[23] *Power Available: Unlocking Renewables' Potential to Help Balance the Electricity System*, Nat. Grid ESO, Warwick, U.K., May 2020.
[24] T. Burton, D. Sharpe, N. Jenkins, and E. Bossanyi, "The wind resource," in *Wind Energy Handbook*. Hoboken, NJ, USA: Wiley, 2003, pp. 11–39.
[25] *Notes on Wind Farm Constraint Payments*, Renew. Energy Found., London, U.K., 2017.
[26] Y. Zhang, J. Bank, Y.-H. Wan, E. Muljadi, and D. Corbus, "Synchrophasor measurement-based wind plant inertia estimation," in *Proc. IEEE Green Technol. Conf. (GreenTech)*, Denver, CO, USA, Apr. 2013, pp. 494–499.
[27] O. Beltran, R. Peña, J. Segundo, A. Esparza, E. Muljadi, and D. Wenzhong, "Inertia estimation of wind power plants based on the swing equation and phasor measurement units," *Appl. Sci.*, vol. 8, no. 12, p. 2413, Nov. 2018.
[28] F. Milano and A. Ortega, "Frequency divider," *IEEE Trans. Power Syst.*, vol. 32, no. 2, pp. 1493–1501, Mar. 2017.
[29] F. Milano and A. Ortega, "A method for evaluating frequency regulation in an electrical grid—Part I: Theory," *IEEE Trans. Power Syst.*, vol. 36, no. 1, pp. 183–193, Jan. 2021.
[30] F. Milano, A. Ortega, and A. J. Conejo, "Model-agnostic linear estimation of generator rotor speeds based on phasor measurement units," *IEEE Trans. Power Syst.*, vol. 33, no. 6, pp. 7258–7268, Nov. 2018.
[31] M. Liu, J. Chen, and F. Milano, "On-line inertia estimation for synchronous and non-synchronous devices," *IEEE Trans. Power Syst.*, vol. 36, no. 3, pp. 2693–2701, May 2021.
[32] C. Phurailatpam, Z. H. Rather, B. Bahrani, and S. Doolla, "Measurement-based estimation of inertia in AC microgrids," *IEEE Trans. Sustain. Energy*, vol. 11, no. 3, pp. 1975–1984, Jul. 2020.
[33] C. Phurailatpam, Z. H. Rather, B. Bahrani, and S. Doolla, "Estimation of non-synchronous inertia in AC microgrids," *IEEE Trans. Sustain. Energy*, early access, Apr. 2, 2021, doi: 10.1109/TSTE.2021.3070678.
[34] A. Fernández-Guillamón, A. Vigueras-Rodríguez, and A. Molina-García, "Analysis of power system inertia estimation in high wind power plant integration scenarios," *IET Renew. Power Gener.*, vol. 13, pp. 2807–2816, Nov. 2019. [Online]. Available: https://arxiv.org/abs/2005.02091
[35] K. Tuttelberg, J. Kilter, and K. Uhlen, "Comparison of system identification methods applied to analysis of inter-area modes," in *Proc. Int. Power Syst. Transients Conf.*, Seoul, South Korea, Jun. 2017, p. 6.
[36] K. Tuttelberg, J. Kilter, D. Wilson, and K. Uhlen, "Estimation of power system inertia from ambient wide area measurements," *IEEE Trans. Power Syst.*, vol. 33, no. 6, pp. 7249–7257, Nov. 2018.
[37] V. Sagar and S. Kumar Jain, "Estimation of power system inertia using system identification," in *Proc. IEEE Innov. Smart Grid Technol.-Asia (ISGT Asia)*, Chengdu, China, May 2019, pp. 285–290.
[38] F. Allella, E. Chiodo, G. M. Giannuzzi, D. Lauria, and F. Mottola, "On-line estimation assessment of power systems inertia with high penetration of renewable generation," *IEEE Access*, vol. 8, pp. 62689–62697, 2020.
[39] B. Tan, J. Zhao, M. Netto, V. Krishnan, V. Terzija, and Y. Zhang, "Power system inertia estimation: Review of methods and the impacts of converter-interfaced generations," *Int. J. Electr. Power Energy Syst.*, vol. 134, Jan. 2022, Art. no. 107362.
[40] A. Junyent-Ferre and O. Gomis-Bellmunt, "Control of power electronic converters for the operation of wind generation systems under grid disturbances," Ph.D. dissertation, Universitat Politecnica de Catalunya, Barcelona, Spain, May 2011.
[41] A. Roscoe, T. Knueppel, R. Da Silva, P. Brogan, I. Gutierrez, D. Elliott, and J. P. Campion, "Response of a grid forming wind farm to system events, and the impact of external and internal damping," *IET Renew. Power Gener.*, vol. 14, no. 19, pp. 3908–3917, Dec. 2020.
[42] W. Hu, Z. Wu, and V. Dinavahi, "Dynamic analysis and model order reduction of virtual synchronous machine based microgrid," *IEEE Access*, vol. 8, pp. 106585–106600, 2020.
[43] *System Identification Toolbox*, MathWorks, Natick, MA, USA, 2020.
[44] A. Rolán, Á. Luna, G. Vázquez, D. Aguilar, and G. Azevedo, "Modeling of a variable speed wind turbine with a permanent magnet synchronous generator," in *Proc. IEEE Int. Symp. Ind. Electron. (ISIE)*, Seoul, South Korea, Jul. 2009, pp. 734–739.
[45] H. Geng, D. Xu, B. Wu, and G. Yang, "Active damping for PMSG-based WECS with DC-link current estimation," *IEEE Trans. Ind. Electron.*, vol. 58, no. 4, pp. 1110–1119, Apr. 2011.
[46] S. D'Arco and J. A. Suul, "Virtual synchronous machines—Classification of implementations and analysis of equivalence to droop controllers for microgrids," in *Proc. IEEE Grenoble Conf.*, Grenoble, France, Jun. 2013, pp. 1–7.
[47] *Load-Frequency Control Annual Report 2018*, ENTSO-E, Brussels, Belgium, Sep. 2019.
[48] C. Broderick, "Rate of change of frequency (RoCoF) withstand capability," ENTSO-E, Brussels, Belgium, Tech. Rep., Jan. 2018.
[49] *Changes to the Distribution Code and Engineering Recommendation G59: Frequency Changes During Large Disturbances and Their Impact on the Total System*, Jul. 2014.
[50] *International Standard Wind Turbines—Part 1: Design Requirements*, Standard IEC 61400-1, International Electrotechnical Commission, Geneva, Switzerland, 2005.
[51] D. Pan, X. Wang, F. Liu, and R. Shi, "Transient stability of voltage-source converters with grid-forming control: A design-oriented study," *IEEE J. Emerg. Sel. Topics Power Electron.*, vol. 8, no. 2, pp. 1019–1033, Jun. 2020.

SAM HARRISON received the M.Sci. degree in oceanography from the University of Southampton, in 2018. He is currently pursuing the Ph.D. degree in electronic and electrical engineering with the Wind and Marine Energy Systems Centre for Doctoral Training (CDT), University of Strathclyde. His research interests include the integration of renewable energy sources, particularly, wind turbine, and power converter control and power system stability.

PANAGIOTIS N. PAPADOPOULOS (Member, IEEE) received the Dipl.Eng. and Ph.D. degrees from the Department of Electrical and Computer Engineering, Aristotle University of Thessaloniki, Greece, in 2007 and 2014, respectively. He is currently a Senior Lecturer and a UKRI Future Leaders Fellow with the Department of Electronic and Electrical Engineering, University of Strathclyde, Glasgow, U.K. His research interests include power system stability and dynamics, focusing on challenges introduced by the increasing uncertainty and complexity in power system dynamic behavior.

RICARDO DA SILVA received the degree in electrical engineering from Simón Bolívar University, Caracas, Venezuela, with specialization in power systems, and the M.Sc. degree in renewable energy and environment from the Polytechnical University of Madrid, in 2012. He is currently pursuing the dual Master of Business Administration degree with Strathclyde University, Glasgow, and Pontificia Comillas University, Madrid, with a focus on the energy sector.

He has experience in electrical engineering and electricity markets from his work in energy utilities in Spain, Ireland, and the U.K., where he is currently a Grid and Regulation Manager at ScottishPower Renewables. His understanding of the power system and its scarcities out of the increase of renewable integration has helped him develop an expertise on system services product design and how to provide signals to facilitate decarbonization of ancillary services markets.

ANTHONY KINSELLA received the M.Eng. degree in mechanical engineering from the University of Strathclyde, Glasgow, U.K., in 2010.

He was a Maintenance Engineer with Gates Corporation from 2010 to 2011. From 2011 to 2013, he was a Reliability Engineer with Weir Engineering Services. In 2013, he moved to The Weir Group PLC as a Technology Analyst and from 2015 to 2018, he was an Open Innovation Manager. In 2018, he moved to ScottishPower Renewables, where he is currently a Prospective Technology Manager in business development.

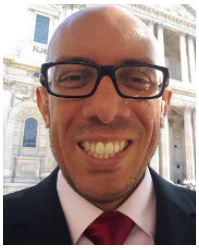

ISAAC GUTIERREZ received the B.Sc. degree in electrical and mechanical engineering from the Department of Electrical Engineering, Technological University of Panama, Panama City, Panama, in 1996, and the M.Sc. and Ph.D. degrees from the Department of Mechanical Engineering, Kanazawa University, Kanazawa, Japan, in 2002 and 2005, respectively.

He is currently a Lead Electrical Engineer for grid integration matters at ScottishPower Renewables, U.K. He has over 20 years of experience in the renewable energy sector. He has been an Active Member of the Grid Code Working Group, U.K., including those on virtual synchronous machines/grid forming and modeling. Most recently, his work has focused on enabling a windfarm to operate in grid forming mode and demonstrate the provision of black start services. His main research interests include ensuring grid code compliance of onshore and offshore windfarms, STATCOM design review, installation, and site testing.

Dr. Gutierrez is a member of the Institution of Engineering and Technology (IET), U.K.

AGUSTI EGEA-ALVAREZ (Member, IEEE) received the B.Sc., M.Sc., and Ph.D. degrees from the Technical University of Catalonia, Barcelona, in 2008, 2010, and 2014, respectively. In 2015, he was Marie Curie Fellow with China Electric Power Research Institute (CEPRI). In 2016, he joined Siemens Gamesa as a Converter Control Engineer, working on grid forming controllers and alternative HVDC schemes for offshore wind farms. He has been a member of the Power Electronics, Drives and Energy Conversion (PEDEC) Group, since 2018. He is currently a Senior Lecturer with the Department of Electronic and Electrical Engineering. His current research interests include the control and operation of high-voltage direct current systems, renewable generation systems, electrical machines, and power converter control.